Physics of the Earth and Planetary Interiors 178 (2010) 80–91

Contents lists available at ScienceDirect

Physics of the Earth and Planetary Interiors

journal homepage: www.elsevier.com/locate/pepi

Steep reflections from the earth's core reveal small-scale heterogeneity in the upper mantle

Hrvoje Tkalčić[a,*], Vernon F. Cormier[b], Brian L.N. Kennett[a], Kuang He[b]

[a] Research School of Earth Sciences, The Australian National University, Mills Road, Jaeger Building 61, Canberra, ACT 0200, Australia
[b] Department of Physics, University of Connecticut, 2152 Hillside Road U-3046, Storrs, CT 06269-3046, United States

ARTICLE INFO

Article history:
Received 25 January 2009
Received in revised form 6 August 2009
Accepted 19 August 2009

Edited by: K. Zhang and M. Bergman.

Keywords:
Inner core
Core–mantle boundary
Seismic body waves
Upper mantle heterogeneity
Scattering

ABSTRACT

We investigate arrivals of seismic phases reflected from the core–mantle boundary (PcP waves) and those reflected from the inner-core boundary (PKiKP waves) at subcritical angles, with the goal of measuring their amplitude ratios. This adds invaluable data points required to study the density jump across the inner-core boundary (ICB). One nuclear explosion and one earthquake, both with favourable focal mechanisms are identified as sources that produce an excellent and abundant record of arrivals of both PcP and PKiKP waves at multiple stations. There is only a limited number of detections of both types of waves on the same seismogram, while more frequently, either one or another of the two phases is detected. Thus, for those cases where at least one phase is above a detectable level, we observe a highly significant negative correlation (anti-correlation) of phase appearances on seismograms, where PcP and PKiKP phase-detections are treated as dichotomous, categorical random variables that can take values detected or undetected. The fact that similar anti-correlation in detection is observed for both explosive and tectonic sources makes less likely the possibility that source effects or a specific near source structure is responsible for this phenomenon. Although laterally varying structure near the core–mantle boundary (CMB) can account for the magnitude of observed fluctuations in the amplitude ratio of PKiKP to PcP, the Fresnel volumes surrounding their ray paths are well separated at the CMB at the frequencies of interest. This separation excludes the possibility that complex structure at or near the CMB is the dominant effect responsible for the observed anti-correlation. We demonstrate that the interaction of the wavefield with near-receiver heterogeneities is an important additional source of amplitude fluctuations across arrays of stations, and the likely cause of the anti-correlation between PKiKP and PcP detections and their spatial coherences at regional arrays. The combined effects of heterogeneities near the surface and the CMB have a profound impact on the estimates of the PKiKP/PcP amplitude ratios and the subsequent estimates of the density jump at the ICB.

1. Introduction and motivation

PKiKP waves have been typically difficult to observe at subcritical distances. It has been argued that arrivals occur only in rare cases, with just enough energy to get barely recorded above noise, and hence only providing estimates of the upper bound of the ICB density jump (e.g., Souriau and Souriau, 1989; Shearer and Masters, 1990). Souriau and Souriau (1989) stated that PKiKP emerges only slightly out of the noise, which may arise from focusing by some heterogeneity. Shearer and Masters (1990) made similar remarks, identifying only one convincing simultaneous arrival of PKiKP and PcP waves on the global scale. Attempts to collect PcP waves globally sometimes reveal very clean reflections of the CMB, but at other times PcP is completely buried in noise or hardly visible (Tkalčić et al., 2002; Tkalčić and Romanowicz, 2002). The existence of high quality PcP arrivals at one station does not guarantee the existence of PcP arrivals on another nearby station of a similar quality. Although this could be attributed to the topography at the CMB and the variability in source radiation pattern, this "patchy" pattern of PcP observations is still not well understood.

Here we present unusually high quality-observations of a large number of PcP and PKiKP phases—from an earthquake and a nuclear explosion. Such high quality records are rare and previously relatively unexploited for the purposes of studying the deep earth. Our primary motivation was to compile a dataset of PcP and PKiKP waves observed on the same seismogram for the purpose of studying the density jump at the ICB. In the course of that study we found that such observations of PcP and PKiKP at a single station were rare, the more common situation being that when PKiKP is observed, PcP is not, and *vice versa*. Observations of PcP and PKiKP waves on the same seismogram, however, could still be used to provide some bounds on the density jump at the ICB (Tkalčić et al.,

* Corresponding author. Tel.: +61 2 6125 3213; fax: +61 2 6257 2737.
E-mail address: Hrvoje.Tkalcic@anu.edu.au (H. Tkalčić).

0031-9201/$ – see front matter © 2009 Elsevier B.V. All rights reserved.
doi:10.1016/j.pepi.2009.08.004

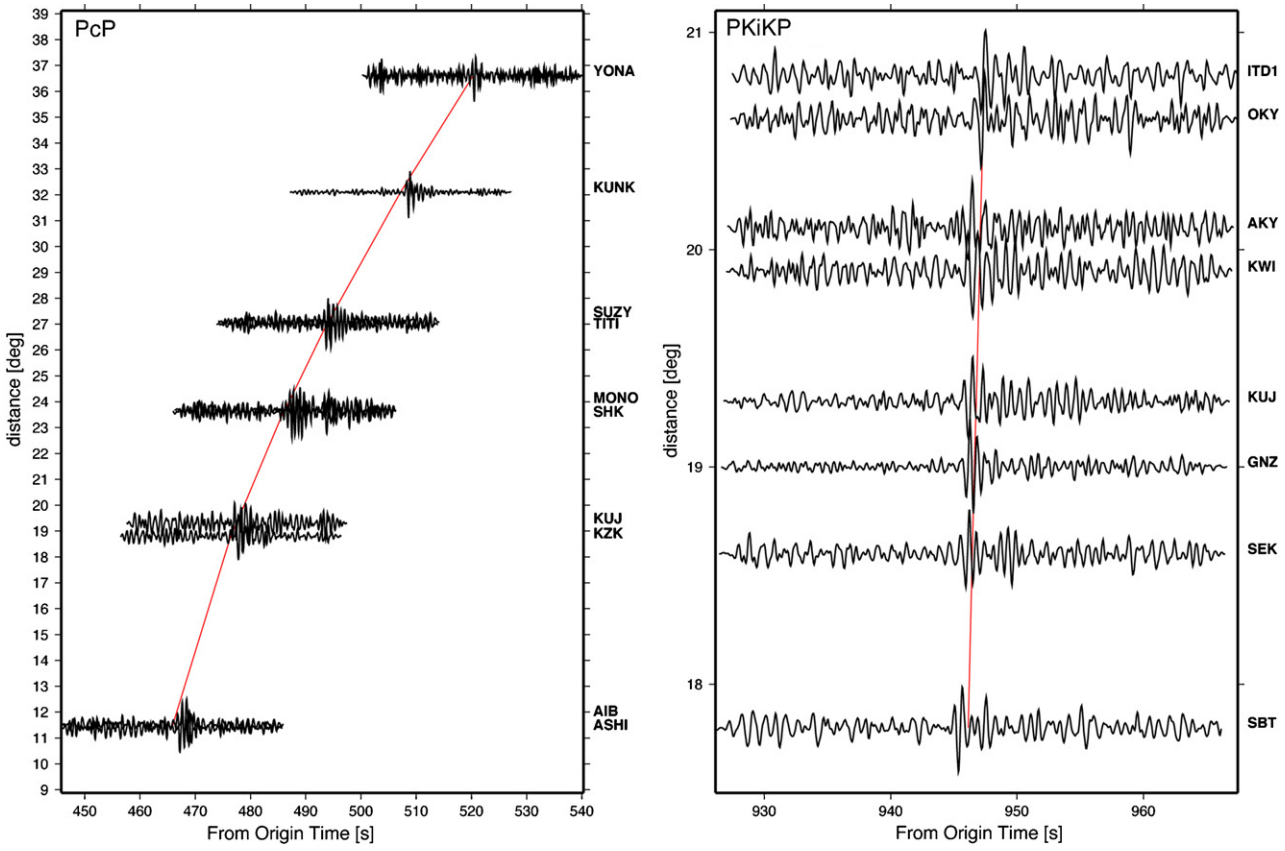

Fig. 1. Selected PcP (left) and PKiKP (right) observations for the $m_b = 5.7$ earthquake located northwest of Kuril Islands and dated 02/07/2001. The broadband velocigrams are bandpass filtered between 1 and 3 Hz. The theoretical travel time prediction of PcP and PKiKP from the ak135 model is shown by solid line. The scales for PcP and PKiKP records are different to account for the space and changing slowness across the range of selected stations.

2009). In this paper, we explore the character and possible causes of the observed anti-correlation in the detection of PcP and PKiKP. Among the potential causes are heterogeneities in both the deep and shallow earth. We come to the conclusion that near-receiver structure is the most likely cause. This conclusion is in agreement with numerous studies of transmission fluctuations across various seismic arrays, dating back to the pioneering study of Aki (1973), which point to small-scale (10s of km and less) heterogeneities in the crust and upper mantle as likely sources of scattering and causes of fluctuations in amplitudes of body waves. Specifically, we demonstrate the probable existence of the phenomenon of angular decorrelation (e.g., Flatté and Wu, 1988; Wu and Flatté, 1990) between PKiKP and PcP waveforms, which sample the heterogeneous structure beneath the receiver at different angles of incidence.

2. Data and the observed anti-correlation in the detection of PKiKP and PcP

We report multiple arrivals of PcP and PKiKP waves from two distinctive events (Figs. 1–4), an explosion and an earthquake. The explosion in Central Asia should have nearly an isotropic radiation pattern for P waves and be less affected by the complex near source structure commonly surrounding a tectonic earthquake. The earthquake in the Kurile arc has a relatively robustly determined focal mechanism. The epicentral distances (10–70°) of the observations span a wide range of ray take-off angles, including nearly vertical angles where the ray paths of PcP and PKiKP are nearly identical in the mantle. Digital waveforms are filtered using consecutive Butterworth bandpass filters of different widths and spectrograms to emphasize and identify the PcP and PKiKP wave arrivals.

The first set of arrivals (Fig. 1) originated from an earthquake north of the Kuril Islands and was recorded at the J-array stations in Japan and several stations on neighboring islands (Fig. 2). A total of 29 records were selected, where either the PcP or PKiKP waves were observed at individual stations. In rare cases, both phases were present on the same seismogram. If the phase is observed, we assign quality A or B for good and C for very weak signals (in only three cases for PcP waves and in one case for PKiKP waves), see Table 1. If one phase is buried in noise and not visible, while the other is visible, quality D for the first phase is assigned. An alternating pattern of detections of PcP and PKiKP waves (one is detected and the other is not) is observed in 24 out of 29 cases. Particularly interesting is the lack of PcP wave arrivals between about 19.6° and 20.8° epicentral distances. There is one simultaneous observation at 23.6°, but beyond this, the PcP wave arrivals take over from 24.6° to 36.7°, while the PKiKP wave arrivals are not visible (Table 1).

The second set of arrivals originated from a nuclear explosion from the Lop Nor test site (Fig. 3). The recording stations are distributed across continental Asia (Fig. 4). A total of 40 records were selected with at least one observation of either or both PcP or PKiKP waves on individual stations. The alternating pattern of detections of PcP and PKiKP waves is observed in 30 out of 39 cases, with one observation excluded because of the unusually late PKiKP arrival. Detections of both PcP and PKiKP waves from 11.7° to 13.4° epicentral distance, as well as two detections at stations ZRN and VOS were used in a separate study to estimate the density jump across the ICB using a new method that incorporates seismic noise (Tkalčić et al., 2009). ZRN at 17.5° is the last station that recorded visible PcP and PKiKP waves, and at larger epicentral distances PKiKP waves are only observed twice more, but each time with the PcP waves buried in noise. The large number of

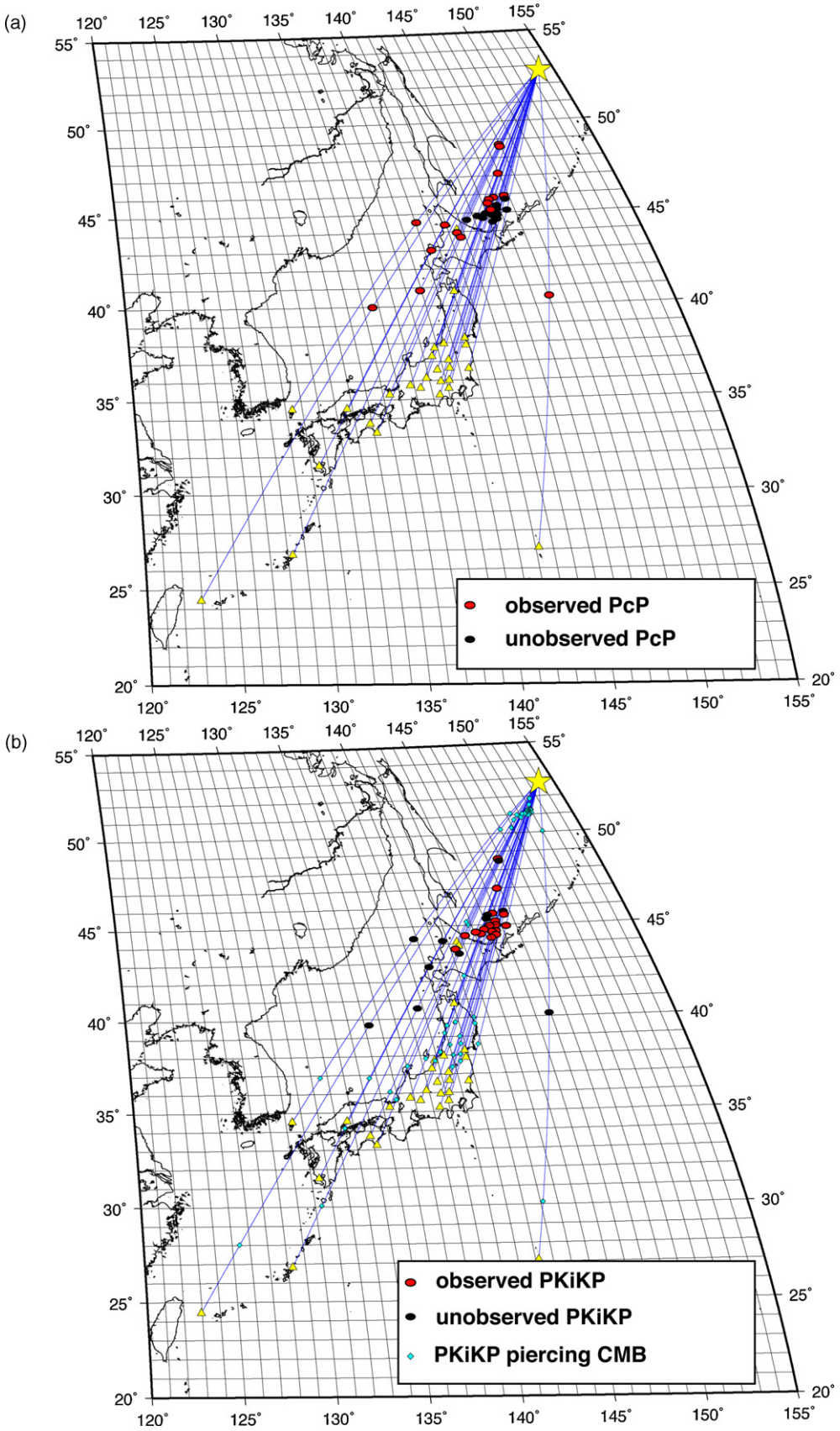

Fig. 2. The $m_b = 5.7$ earthquake located northwest of Kurile Islands and dated 02/07/2001 (star), and the stations from Table 1 (triangles). Surface-projections of ray paths are shown in solid lines. (a) The observed PcP waves are indicated as red ellipses plotted as the bottoming points of the PcP waves at the core–mantle boundary. The unobserved PcP waves are shown by black ellipses. (b) The observed PKiKP waves are indicated as red ellipses plotted as the bottoming points of the PKiKP waves at the inner-core boundary. The unobserved PKiKP waves are shown by black ellipses. Also shown are the piercing points of the PKiKP waves at the core–mantle boundary (light blue diamonds). (For interpretation of the references to color in this figure legend, the reader is referred to the web version of the article.)

Table 1
Observations of PcP and PKiKP waves for the Kuril Islands earthquake dated 01/02/07 and a Lop Nor test-site explosion dated 94/10/07. Amplitude displacement measurements in counts are indicated under A for PcP and B for PKiKP. If the arrivals are visible (mainly quality A or B) or very weak (quality C), this is indicated by "signal", while if they are buried in noise (quality D), this is indicated by "NOISE" (under OBS1 for PcP and OBS2 for PKiKP). The PKiKP/PcP ratio is calculated, along with the PKiKP/P and PcP/P waves ratio. Observe the anti-correlation patter between "signal" and "NOISE" markers, with the exception of simultaneous observations.

Event/yymmdd	Station	Distance [°]	OBS1	A (PcP) [counts]	Quality	OBS2	B(PKiKP) [counts]	Quality	B/A	A/P	B/P
010207	ASHI	11.35	signal	86.579	A	signal	28.081	A	0.324	0.028	0.088
010207	AIB	11.50	signal	17.749	A	NOISE	3.560	D	0.201	0.032	0.157
010207	ERIM	12.88	NOISE	74.352	D	early	9999	B	9999	9999	0.069
010207	TNMA	14.74	signal	112.859	B	signal	25.386	A	0.225	0.030	0.130
010207	AOB	17.03	signal	115.525	B	NOISE	6.058	D	0.052	0.014	0.258
010207	MARU	17.39	NOISE	103.810	D	signal	16.733	B	0.161	0.022	0.137
010207	SBT	17.80	signal	21.711	C	signal	2.045	A	0.094	0.012	0.131
010207	YHJ	18.26	signal	17.466	B	NOISE	3.746	D	0.214	0.025	0.116
010207	SEK	18.56	NOISE	10.340	D	signal	1.493	A	0.144	0.015	0.103
010207	HIT	18.57	NOISE	33.080	D	signal	3.091	B	0.093	0.025	0.263
010207	KZK	18.75	signal	29.523	A	NOISE	2.157	D	0.073	0.025	0.341
010207	GNZ	18.97	NOISE	4.144	D	signal	1.003	A	0.242	0.035	0.145
010207	KUJ	19.34	signal	32.197	B	signal	3.903	A	0.121	0.033	0.270
010207	DDR	19.63	NOISE	9.848	D	signal	0.385	B	0.039	0.016	0.419
010207	KWI	19.88	NOISE	13.942	D	signal	1.306	A	0.094	0.006	0.069
010207	ASI	20.03	NOISE	11.550	D	signal	1.064	B	0.092	0.029	0.313
010207	AKY	20.06	NOISE	25.532	D	signal	2.456	B	0.096	0.014	0.147
010207	OKY	20.60	NOISE	14.321	D	signal	2.372	A	0.166	0.015	0.089
010207	KURK	20.69	NOISE	43.429	D	signal	7.163	C	0.165	0.013	0.076
010207	ITD1	20.80	NOISE	13.130	D	signal	1.895	A	0.144	0.008	0.056
010207	WACH	21.76	NOISE	39.883	D	signal	10.350	B	0.260	0.033	0.127
010207	SHK	23.59	signal	12.128	B	NOISE	3.434	D	0.283	0.045	0.159
010207	MONO	23.74	signal	84.315	A	signal	18.683	A	0.222	0.080	0.363
010207	MRMJ	24.03	signal	5.242	C	NOISE	3.018	D	0.576	0.159	0.277
010207	TUSI	25.14	signal	59.725	C	NOISE	30.408	D	0.509	0.215	0.422
010207	TITI	27.02	signal	199.914	A	NOISE	48.079	D	0.240	0.104	0.433
010207	SUZY	27.14	signal	58.304	A	NOISE	13.911	D	0.239	0.092	0.387
010207	KUNK	32.12	signal	243.076	A	NOISE	31.340	D	0.129	0.016	0.127
010207	YONA	36.61	signal	260.963	A	NOISE	106.959	D	0.410	0.594	1.449
941007	UCH	10.64	NOISE	53.818	D	signal	3.904	B	0.073	0.005	0.075
941007	SP01	10.92	signal	71.998	A	late	9999	A	9999	9999	0.251
941007	KUR	11.49	NOISE	3526.123	D	signal	123.861	B	0.035	0.012	0.329
941007	BB08	11.55	NOISE	6.167	D	signal	4.516	A	0.732	0.045	0.062
941007	BB10	11.67	signal	9.872	A	signal	2.420	A	0.245	0.057	0.234
941007	BB36	11.88	signal	16.604	A	signal	1.696	B	0.102	0.036	0.355
941007	BB14	12.27	signal	24.051	A	signal	1.464	B	0.061	0.008	0.131
941007	BB18	12.68	signal	15.942	A	signal	1.959	B	0.123	0.018	0.144
941007	BB20	12.88	signal	63.145	A	signal	17.091	A	0.271	0.153	0.566
941007	BB23	13.12	signal	34.057	A	signal	3.804	A	0.112	0.046	0.411
941007	SP25	13.41	signal	48.009	A	signal	6.600	B	0.137	0.020	0.147
941007	SP27	13.91	NOISE	38.251	D	signal	13.851	A	0.362	0.036	0.101
941007	VOS	16.37	signal	3552.208	B	signal	200.452	A	0.056	0.015	0.257
941007	BRVK	16.91	NOISE	29.065	D	signal	3.245	B	0.117	0.015	0.130
941007	CHK	17.12	NOISE	2580.993	D	signal	223.173	A	0.086	0.006	0.074
941007	ZRN	17.49	signal	2463.003	B	signal	159.492	A	0.065	0.011	0.167
941007	AKT	22.96	signal	193.611	A	NOISE	12.642	D	0.065	0.020	0.306
941007	ARU	24.47	signal	33.167	A	NOISE	5.598	D	0.169	0.026	0.151
941007	CHTO	24.36	signal	6.870	B	NOISE	3.443	D	0.501	0.046	0.092
941007	YAK	31.73	signal	59.996	B	NOISE	40.377	D	0.673	0.038	0.056
941007	MAJO	38.30	signal	45.254	A	NOISE	4.638	D	0.102	0.070	0.680
941007	YSS	38.38	signal	32.246	B	NOISE	14.258	D	0.442	0.238	0.538
941007	LVZ	38.85	signal	66.882	A	NOISE	10.535	D	0.158	0.167	1.063
941007	TSK	39.84	signal	12.331	A	NOISE	2.612	D	0.212	0.121	0.572
941007	MA2	41.53	signal	104.310	A	NOISE	16.713	D	0.160	0.055	0.342
941007	ANTO	41.80	signal	37.316	B	NOISE	5.746	D	0.154	0.052	0.340
941007	KEV	41.95	NOISE	34.050	D	signal	14.126	B	0.415	0.082	0.198
941007	BGIO	43.55	signal	21.751	C	NOISE	11.293	D	0.519	0.009	0.017
941007	OGS	45.76	signal	8.800	B	NOISE	3.432	D	0.390	0.472	1.209
941007	KEG	46.87	signal	87.078	A	NOISE	14.137	D	0.162	0.010	0.059
941007	MORC	48.68	NOISE	6.407	D	signal	2.323	B	0.363	0.064	0.176
941007	DPC	49.18	signal	17.800	A	NOISE	0.945	D	0.053	0.015	0.277
941007	STU	54.13	signal	21.138	B	NOISE	3.945	D	0.187	0.082	0.438
941007	ESK	58.12	signal	86.488	B	NOISE	25.414	D	0.294	0.065	0.222
941007	KOMO	65.41	signal	18.573	B	NOISE	1.407	D	0.076	0.020	0.265
941007	KIBE	66.08	signal	19.179	B	NOISE	1.925	D	0.100	0.026	0.263
941007	KOND	66.81	signal	12.779	B	NOISE	1.728	D	0.135	0.024	0.179
941007	MTOR	67.32	signal	16.954	B	NOISE	1.541	D	0.091	0.014	0.155
941007	MBWE	67.79	signal	13.772	B	NOISE	2.456	D	0.178	0.062	0.347
941007	RUNG	69.82	signal	16.409	B	NOISE	1.512	D	0.092	0.020	0.217

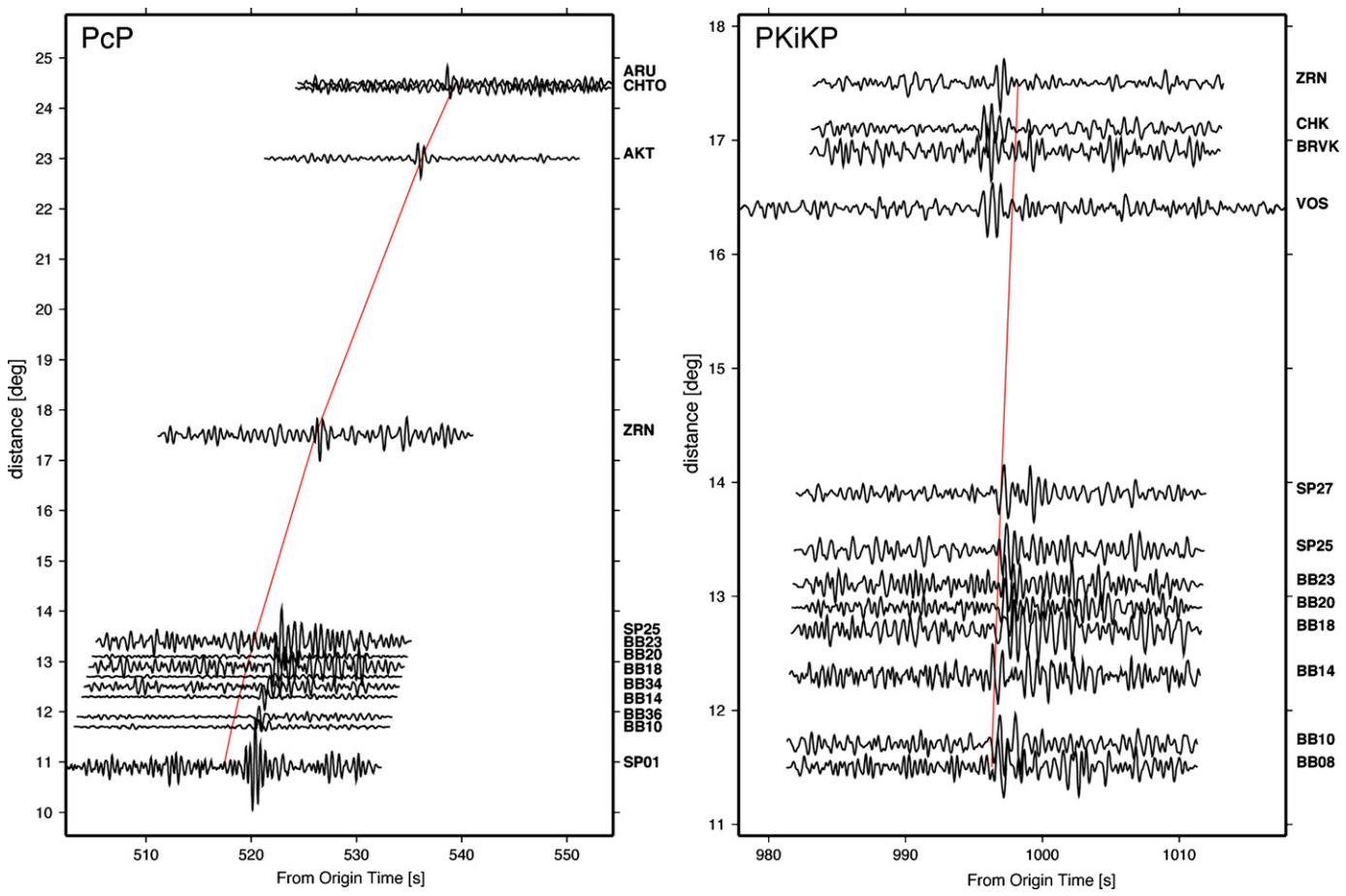

Fig. 3. Same as Fig. 1, but for the $M = 5.9$ explosion located at the Lop Nor test site and dated 10/07/1994.

alternating detections of PcP and PKiKP waves is, again, striking (Table 1).

Table 1 shows the results of the amplitude measurements for PcP and PKiKP waves along with the quality, and indicates whether the arrivals were observed or not for both PcP and PKiKP waves. If the arrivals were not observed, the word "NOISE" is indicated; if the arrivals were observed, the word "signal" is used. It should be noted that Table 1 represents only those seismograms for which at least one of the two phases was detected. Apart from data shown in Table 1, there were 63 seismograms corresponding to other available stations on which there were no detections (see Fig. 7). We took all available data into account, and performed a chi-squared statistical test (χ^2). We tested the null-hypothesis that the distribution of detections of PKiKP waves when PcP is observed on the same seismogram does not differ from the distribution of detections of PKiKP when PcP is not observed. If the null-hypothesis is true, we can establish that the detection of PKiKP waves does not depend on the detection of PcP waves. We defined two categorical, binary random variables ("Detection of PKiKP"; "Detection of PcP"), with two types of data: "yes" and "no". The computed χ^2 statistic does not exceed the critical value for a conventionally accepted 0.05 probability level (in this case, $0.5 < P < 0.1$), therefore we except the null-hypothesis and conclude that the distributions are equal, i.e. that the detection of PKiKP waves is independent on whether or not PcP waves are observed on the same seismogram.

Because of the large number of records on which PcP and PKiKP waves are buried in noise, the above statistics will not reveal if there is a correlation between the detections of PcP and PKiKP waves. Therefore, we repeated the χ^2 statistical test, but now taking into account only those data for which at least one of the two phases was

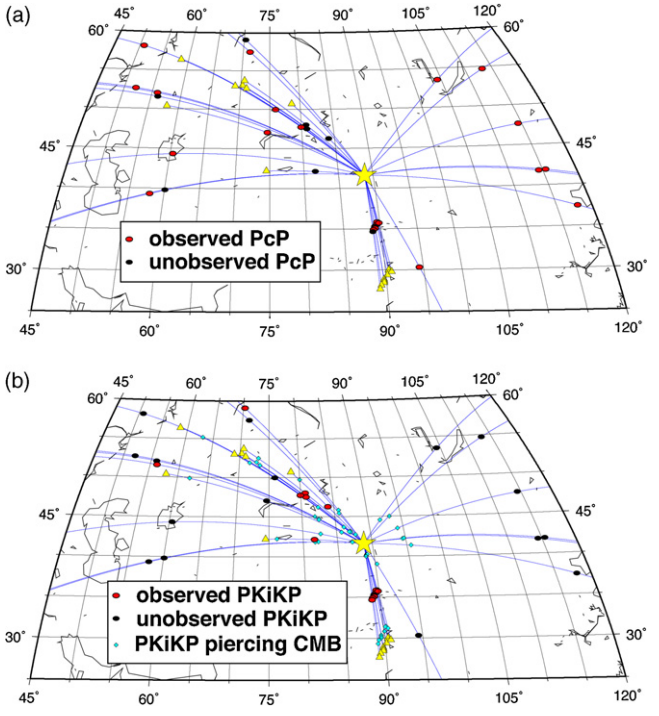

Fig. 4. Same as Fig. 2, but for the $M = 5.9$ explosion located at the Lop Nor test site and dated 10/07/1994.

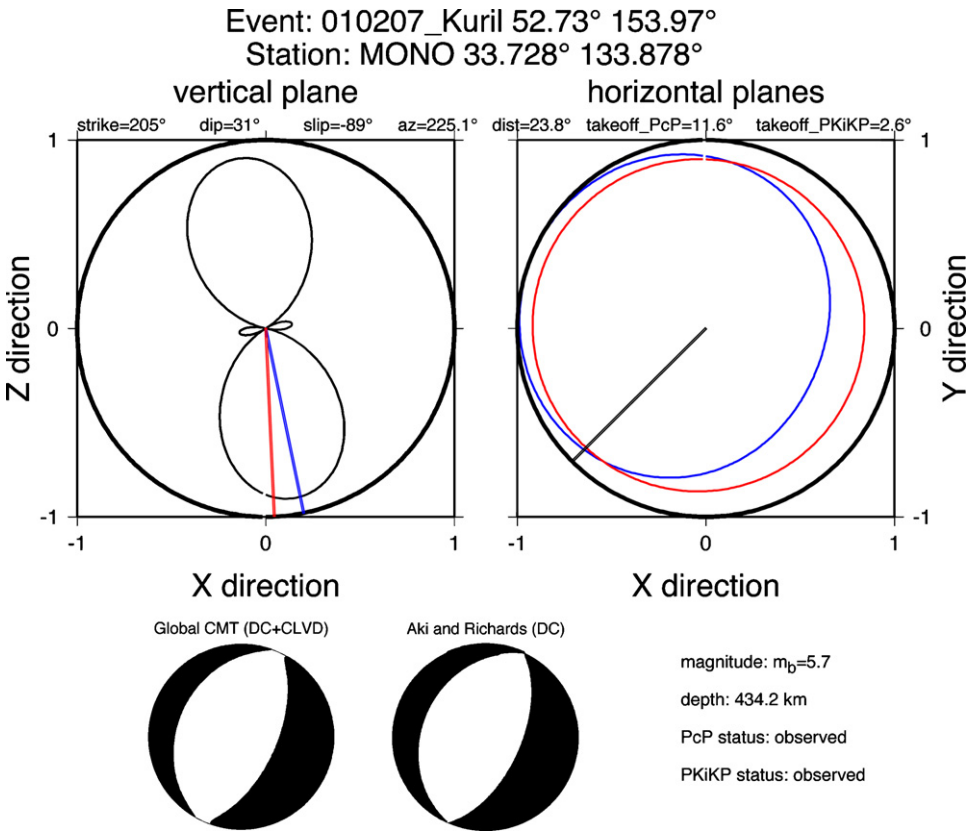

Fig. 5. P-wave energy radiation pattern (black solid lines) for the $m_b = 5.7$ earthquake from Fig. 1, based on the information provided in the global CMT catalogue for the station MONO. Vertical plane is shown on the left, and horizontal plane on the right. Theoretical incident angles of PcP and PKiKP from the ak135 model are shown in blue and red solid lines on the left. The corresponding horizontal cross-sections are shown on the right for PcP (blue) and PKiKP (red). Focal mechanisms with different decomposition of the seismic moment tensor are also shown in the lower left. (For interpretation of the references to color in this figure legend, the reader is referred to the web version of the article.)

detected, making an assumption that both PcP and PKiKP amplitudes are above the detection level. The computed χ^2 statistic now highly exceeds the critical value for 0.05 probability level, therefore we reject the null-hypothesis. The two statistical distributions are not equivalent. Thus the detection of PKiKP waves is dependent on the detection of PcP waves, i.e. if PcP is observed, PKiKP is not, and *vice versa*. We hence confirm the significant negative correlation of the PcP and PKiKP detections (anti-correlation) apparent in Table 1. Out of 67 measurements where at least one of the phases was detected, the alternating pattern of PcP and PKiKP detections is observed on 53 records (79.1%).

3. Possible sources of the anti-correlation

3.1. The radiation pattern

Fig. 5 shows the P-wave radiation pattern for the Kuril Islands earthquake reported in Table 1, for station MONO, at 23.8° epicentral distance. Both vertical- and horizontal-plane cross-sections are shown. Although the difference in take-off angle between PcP and PKiKP waves is 9°, according to the Global CMT solution, these two phases leave the focal sphere with very similar amplitudes, near the maximal values of the radiation pattern. For this particular orientation of the source radiation pattern, no significant variations in the PcP and PKiKP amplitudes are expected. As the epicentral distance increases, the difference increases, although the observations for the earthquake reported in Table 1 do not exceed 36.6°. The P-wave radiation pattern for the explosion reported in Table 1 is expected to be isotropic and therefore it should not affect the amplitudes of PcP and PKiKP waves even at larger epicentral distances. One exception occurs if the explosion radiation is not uniform and contains a spall component. Modeling experiments assuming an additional vertically oriented CLVD source up to half the reported scalar moment of the event, indicate that it is not possible to produce a sufficiently rapid change of radiation pattern over the take-off angle difference between the PKiKP and PcP phase to strongly affect their relative amplitudes.

3.2. Fundamental detectability from ray theoretical amplitudes

Fig. 6 compares the relative ray theoretical amplitudes of PcP and PKiKP as a function of distance in PREM, and PREM per-

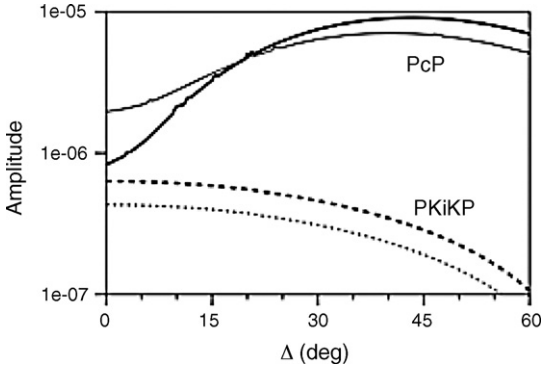

Fig. 6. Comparison of absolute amplitudes of PKiKP and PcP computed from synthetic seismograms of bandpassed particle velocity in PREM (thick solid and thick dashed lines) and in PREM perturbed by an ultra-low velocity zone and low Q zone in the lowermost mantle (thin solid and thin dashed lines).

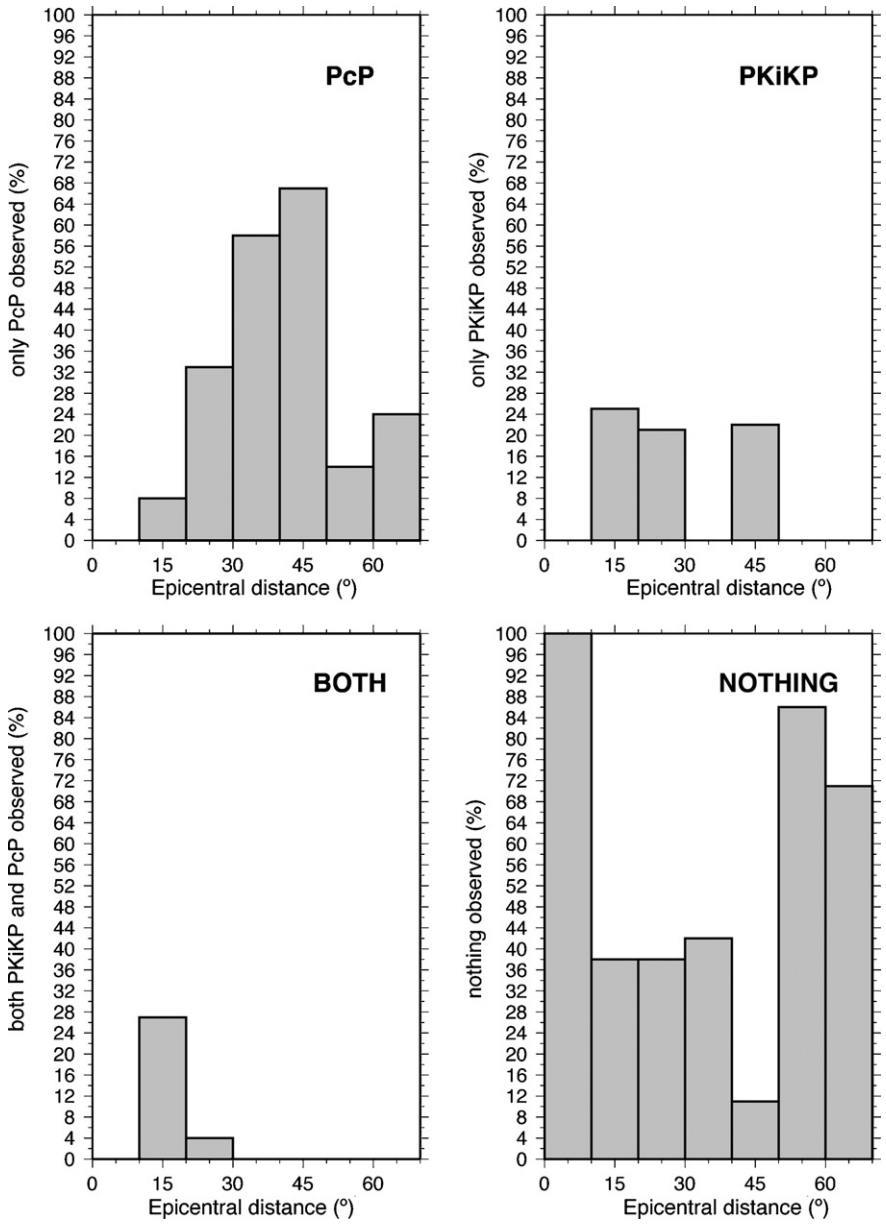

Fig. 7. Histograms showing percentages of observations as function of distance of PcP only, PKiKP only, both PKiKP and PcP, and nothing.

turbed by ultra-low velocity and high attenuation zones near the core–mantle boundary. The distance behavior of theoretical PcP and PKiKP amplitudes in standard earth models with plausible lateral variations near the CMB agrees well with the histograms of observations shown in Fig. 7. Observations in which only PcP is detectable grow strongly in number between 0° and 40°, as does the predicted amplitude of PcP. The percent of observations in which only PKiKP is detectable are fewer in number with no discernible increase or decrease between 15° and 45°, in agreement with the much weaker predicted amplitude of PKiKP relative to PcP and its more gradual dependence on distance. Observations in which both PcP and PKiKP are detected are concentrated at the shortest distance ranges, where the relative amplitudes of the two phases differ by no more than factors of 2–5. The percent of observations in which neither PKiKP nor PcP is detected has no simple trend with distance and simply reflects noise amplitude overwhelming both of these weak phases.

3.3. Heterogeneous structure

PKiKP and PcP waves interact with two regions of increased heterogeneity in 100–400 km thick regions beneath the surface and above the core–mantle boundary (Fig. 8), which have been documented to exist over a broad spectrum of scale lengths from tomographic imaging, and the analysis of high frequency coda (e.g., Li and Romanowicz, 1996; Sato and Fehler, 1998; Cormier, 2000). In the following sub-sections we assess the possibility of either or both of these regions as the contributor to observed anti-correlation between PKiKP and PcP detections.

3.3.1. The core–mantle boundary structure

Considering the spatially clustered behavior of the anti-correlation between PKiKP with PcP detections from their surface projected reflections north of Hokkaido (Fig. 2), it is tempting to hypothesize that small-scale (<50 km) structure at or near the CMB may cause the observed anti-correlation. The points in this cluster

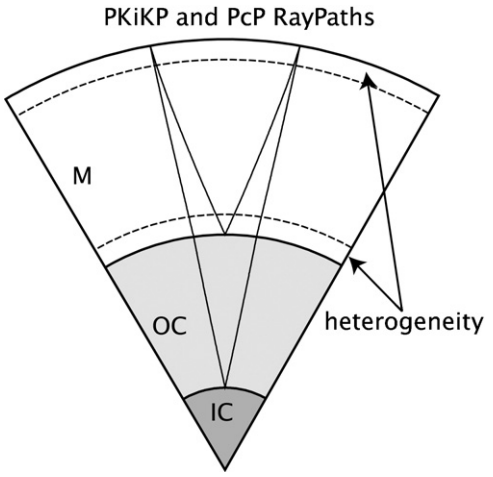

Fig. 8. Ray paths of PKiKP and PcP at 20° great circle distance and their interaction with regions of stronger heterogeneity power in the uppermost and lowermost mantle.

are surface projections of the ICB reflection point of PKiKP and the CMB reflection point of PcP. At the CMB the 1–2 Hz Fresnel volumes for structural sensitivity surrounding PKiKP and PcP rays are separated by more than 200 km for ranges greater than 10° (Fig. 9). Hence, it would require a fortuitous heterogeneity spectrum near the core–mantle boundary to reproduce the observed consistency of the anti-correlation between PKiKP and PcP. The Fresnel volumes of PKiKP and PcP begin to converge beneath the source and receiver, and the tight cluster of reflection points north of Hokkaido corresponds to a tight cluster of receivers on Honshu. These facts suggest that a more likely explanation of the anti-correlation lies with effects of heterogeneity in the crust and upper mantle rather than near the core–mantle boundary. We discuss this possibility in greater detail in a following sub-section.

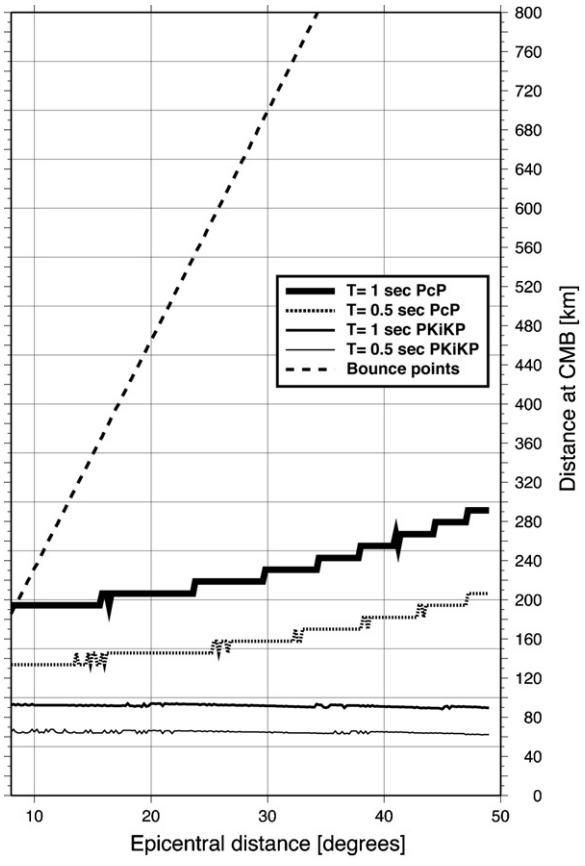

Fig. 9. The Fresnel zone diameter at the core–mantle boundary for the PcP waves (for 1 s period in thick solid line and for 0.5 s period in dotted line) and PKiKP waves (for 1 s period in solid line of medium thickness and for 0.5 s period in thin solid line) as a function of epicentral distance. Also shown is the separation between the PcP bounding and PKiKP piercing points at the core–mantle boundary (dashed line). Spikes in the curves are due to numerical effects.

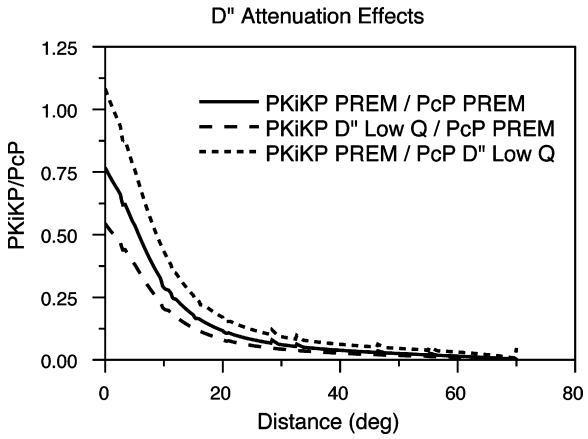

Fig. 10. Effects on the PKiKP/PcP amplitude ratio of a low Q zone ($Q\alpha = 100$) in the lowermost 150 km of the mantle sampled by PKiKP or PcP or both.

Although small-scale structure near the CMB cannot explain the anti-correlation of PKiKP with PcP, larger scale CMB structure (>200 km) may be a significant factor in explaining the variations seen in the measured PKiKP/PcP amplitude ratios. Results of dynamic ray tracing experiments (e.g., Červený, 2001; dynamic ray tracing code by Cormier, 1986) in which either PKiKP, PcP, or both sample a low Q region (Fig. 10), a low velocity region (Fig. 11), or both (Fig. 12) near the CMB predict a variation in the PKiKP/PcP ratio that closely matches the size and range dependence of observed ratios (Fig. 12). These experiments assume a magnitude of lateral variations in lower mantle P velocity and attenuation obtained from global studies of seismic waves grazing the CMB (e.g., Thorne and Garnero, 2004). A lateral variation of P velocity of as little as ±5% concentrated near the CMB combined with a lateral variation in either viscoelastic or scattering attenuation ($1/Q_\alpha$ between 0 and 0.01) in the lowermost 150 km of the mantle can explain most of the scatter seen in the PKiKP/PcP measurements (Fig. 12). Comparison of observed versus predicted PKiKP/PcP ratios due to CMB region structural variations also suggests that an ubiquitous existence of zones of low velocity and high attenuation at the CMB will

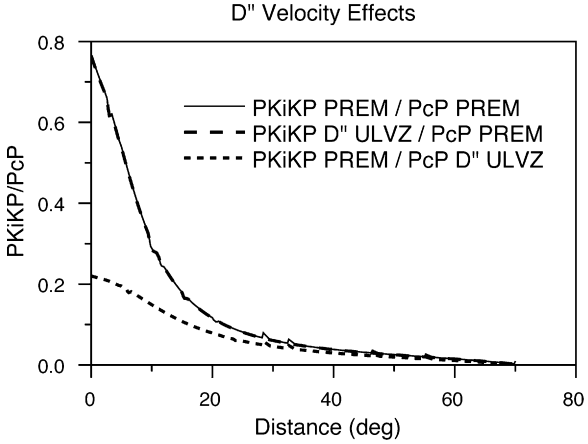

Fig. 11. Effects on the PKiKP/PcP amplitude ratio of a 10% reduction (ULVZ) in P velocity on the mantle side of the core–mantle boundary sampled by PKiKP or PcP, or both.

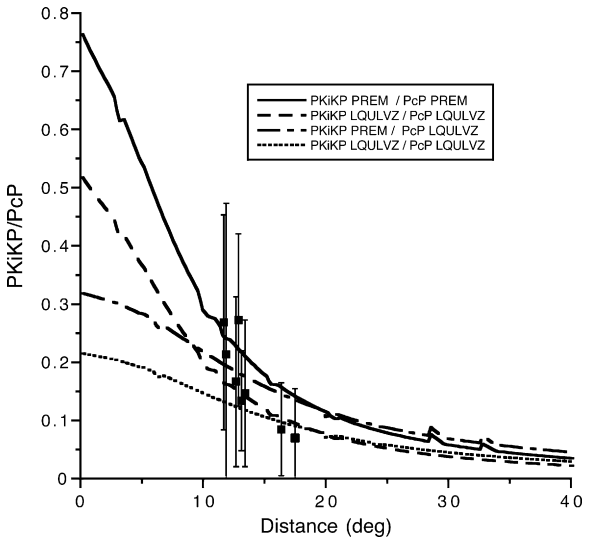

Fig. 12. Combined effects on the PKiKP/PcP amplitude ratio of a low Q zone and ultra-low velocity zone in the lowermost mantle sampled by PKiKP or PcP or both. Measured amplitude ratios (Tkalčić et al., 2009) with estimated error bars plotted with square symbols.

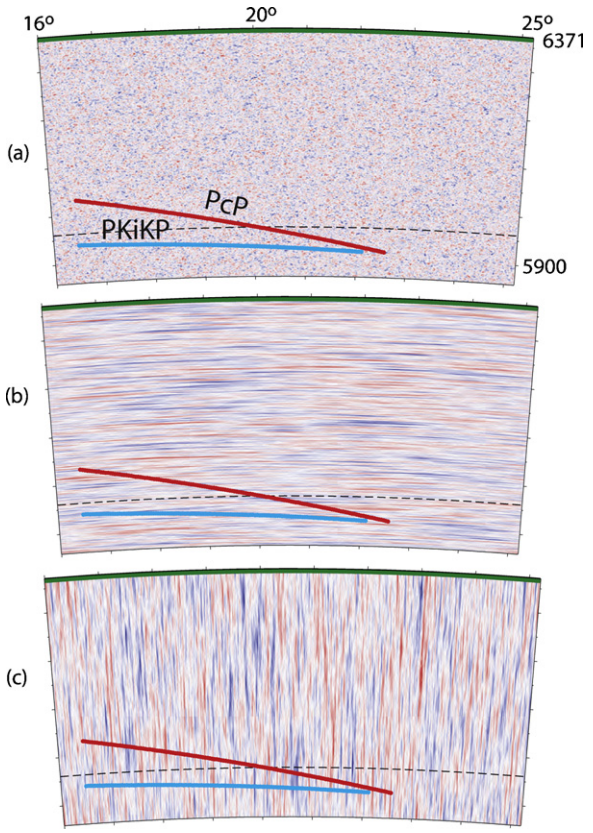

Fig. 13. Wavefronts of PcP (blue) and PKiKP (red) in the range 16–25 incident on an earth model perturbed by statistically described heterogeneity in the crust and upper mantle beneath a receiver array. A 5% RMS perturbation in P velocity is assumed in each case (a–c) with an exponential autocorrelation. (a) Isotropic distribution of scale lengths with a cutoff at 2 km; (b) anisotropic scale distribution of scale lengths with a horizontal cutoff at 100 km and vertical cutoff at 2 km; (c) anisotropic distribution of scale lengths with a vertical cutoff at 100 km and horizontal cutoff at 2 km. (For interpretation of the references to color in this figure legend, the reader is referred to the web version of the article.)

tend to bias estimates of the density jump at the ICB toward lower values. This bias can potentially be minimized using constraints on the structure near PcP CMB reflection points and PKiKP CMB piercing points obtained from independent seismic data sampling these regions.

In addition to volumetric heterogeneity near the CMB, the effects of CMB topography may potentially add to the magnitude of the fluctuation of PcP amplitudes, with an associated smaller effect on PKiKP transmitted back and forth through the CMB. Topography on the CMB been estimated to be on the order of 3 km at scale lengths of 1000s of kilometers (e.g., Sze and Van der Hilst, 2003) and on the order of several 100 m at scale lengths of 10–100 km (Menke, 1986). At the longer scale lengths, the height of the estimated topography is too small to focus or defocus PcP or PKiKP ray paths. At the shorter scale lengths 10–100 km, the Fresnel zones of 1 Hz PcP and PKiKP are wide enough to average over the small effects of 100 m high topography.

3.3.2. *Heterogeneity near the source and receiver*

Either volumetric heterogeneity or topography of a discontinuity near the source can produce large changes in ray direction and potentially affect geometric spreading, but ray theory cannot be used to accurately predict both the effects of wavefront healing and near-field source effects. Instead, either a fully numerical or a hybrid numerical/approximate technique must be used to model the wavefield throughout the whole earth. From elastic reciprocity, the effects of heterogeneity near either the source or receiver will be similar for body waves observed at either arrays of sources or arrays of receivers. Hence, to avoid problems associated with the description of the source, we have chosen to simply model the effects of increased heterogeneity beneath the receivers.

We have used a 2D pseudospectral method (Cormier, 2000) to numerically synthesize the wavefield associated with either a PKiKP or PcP plane wave incident at an array of receivers. The effects of 2D heterogeneity specified by three different spectra of scale lengths were considered (Fig. 13a–c), having either an isotropic or anisotropic distribution of scale lengths specified by a Gaussian autocorrelations of P wave velocity having 5% rms fluctuation. We took spatial and temporal grids with $\Delta x = \Delta z = 0.5$ km and $\Delta t = 0.0135$ s; scaling of P velocity, S velocity, and density variations to be $\Delta V_S/V_S = 2\Delta V_P/V_P$, and $\Delta\rho/\rho = 0$. Point sources were distributed at neighboring grid points to simulate PKiKP (126 points) and PcP (136) plane waves arriving at a receiver array whose center is 20° from the source. A Gaussian far-field displacement source time function was assumed having a half width of 0.18 s, to simulate the typical frequency content of the observations of bandpassed particle velocity. Displacement to particle velocity and 2D line to 3D point source corrections were applied. Seismograms were synthesized in the homogeneous background model to check for the stability of amplitudes and any waveform distortion induced by numerical effects. This test found that amplitude fluctuations at the receiver array were less than a few percent in the homogeneous background medium and waveforms visually agreed with those predicted by ray theory. Figs. 14–16 summarize the effects of peak-to-peak amplitude fluctuations at the receiver array measured from synthetics for PKiKP and PcP incident plane waves for the three types of heterogeneity spectra or textures shown in Fig. 13. The PKiKP/PcP ratios shown in these figures show only the effect of heterogeneity beneath the receiver array and are not corrected for the effects of transmission, reflection, and geometric spreading beneath the zone of heterogeneity, which would significantly reduce the value of the ratio due to the larger absolute amplitude of PcP compared to PKiKP predicted by ray theory in the distance range around 20°. In cases where one phase is detected and the other is not, these simulations illustrate that the spatial coherence of detections or non-detections at dense arrays of receivers (e.g., Figs. 2 and 4) may be simply explained by heterogeneity beneath the receiver.

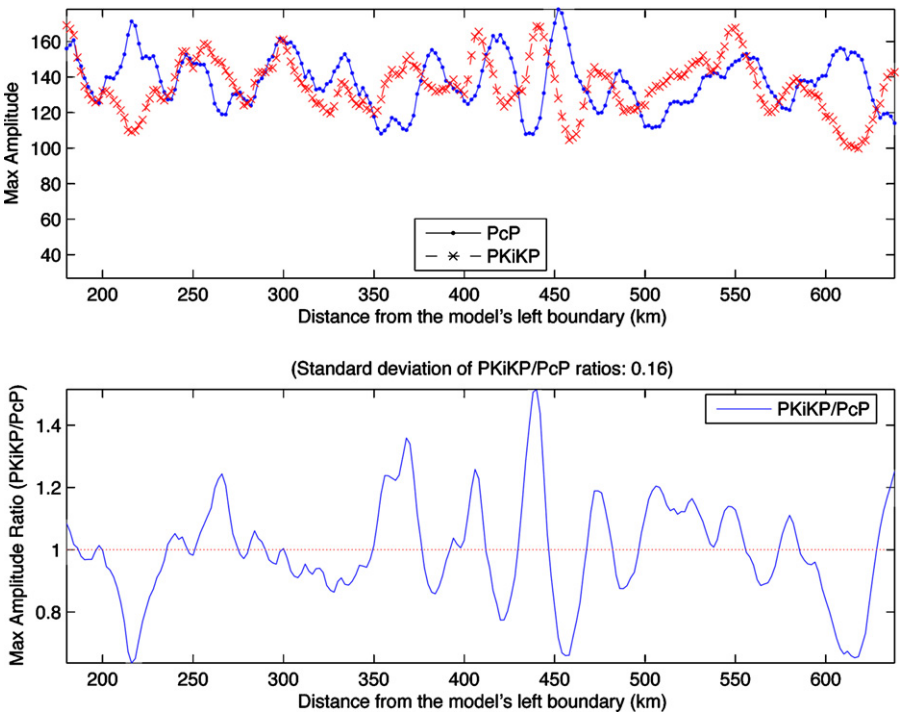

Fig. 14. Predicted amplitude fluctuations of PKiKP and PcP at an array of surface receivers measured from bandpassed seismograms of particle velocity synthesized by a numerical pseudospectral method in the isotropic texture of crust and upper mantle heterogeneity shown in Fig. 13a. The PKiKP/PcP ratio includes only the effects of heterogeneity beneath the receiver array; the effects of differing geometric spreading, viscoelastic attenuation, and reflection/transmission coefficients in deep structure are not included in the PKiKP/PcP ratio.

The simulations in Figs. 14–16 are in qualitative agreement with recent calculations using the phase screen method by Zheng and Wu (2008). They calculated the lateral coherence between the logarithms of amplitudes of two different, near vertically incident, plane waves transmitted through a heterogeneous upper mantle. They found that for plane waves separated by as little as 5° in vertical incidence the coherence of log amplitudes decreases by a factor of 2 at zero lag. This result was predicted at receiver arrays underlain by a 300 km zone of heterogeneity having a Gaussian correlation function with a scale length of 10 km and 1% rms perturbation in P velocity. Scale lengths of this order have long been posed as an explanation of amplitude fluctuations of body waves observed at short-period arrays (e.g., Aki, 1973).

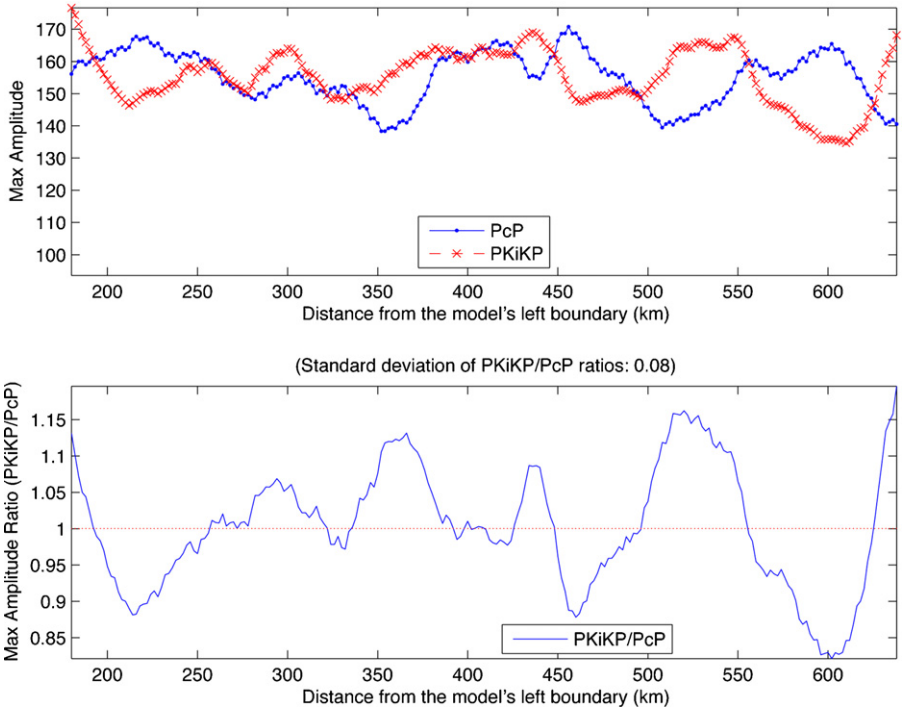

Fig. 15. Same as Fig. 14 but for the anisotropic texture of crust and upper mantle heterogeneity shown in Fig. 13b (horizontal scale lengths longer than vertical scale lengths).

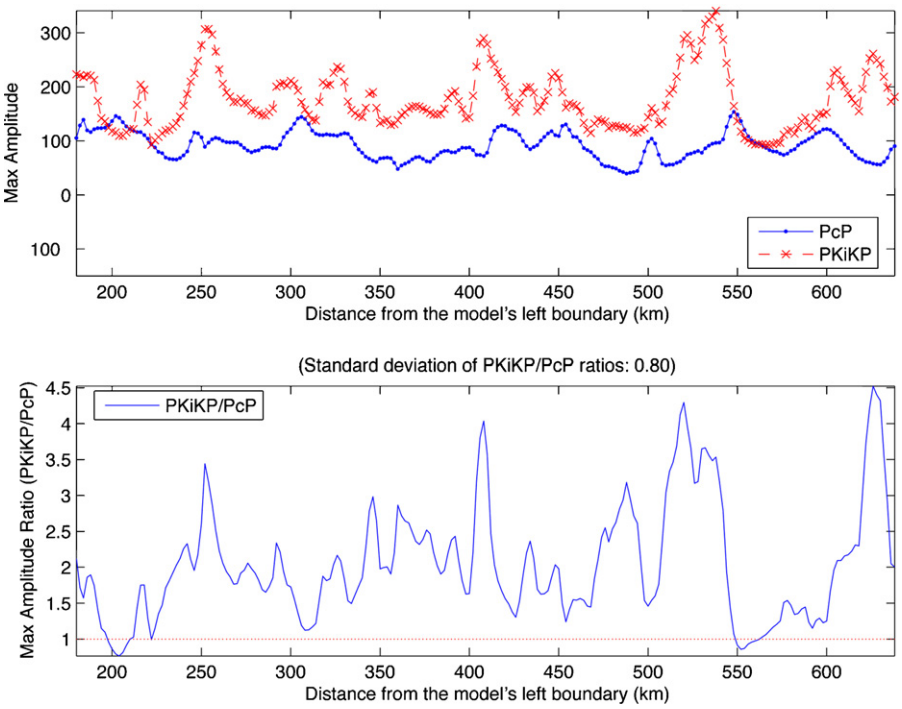

Fig. 16. Same as Fig. 14 but for the anisotropic texture of crust and upper mantle heterogeneity shown in Fig. 13c (vertical scale lengths longer than horizontal scale lengths).

Since the signal to noise ratio of our PcP and PKiKP observations in the cases where one phase is observed and the other is not is often a factor of 2 or less, very similar types of heterogeneity models can easily explain our observed negative correlation between the PKiKP and PcP detections. In the case of an isotropic distribution of scale lengths (Fig. 14), focusing and defocusing of PKiKP is about equally likely to be correlated or uncorrelated with focusing and defocusing of PcP. In the case of horizontally stretched heterogeneity (Fig. 15), focusing and defocusing of PKiKP seems to be generally more anti-correlated with the focusing and defocusing of PcP. In the case of vertically stretched heterogeneity (Fig. 16), PcP is more attenuated by energy lost to backscattering compared to PKiKP. This type of heterogeneity, i.e. one in which quasi-vertically stretched heterogeneity is at a larger angle with respect to the ray normal of the incident PcP wavefront than to the ray normal of the incident PKiKP wavefront, may explain our more exceptional observations in which PKiKP is detected in the 20–40° range but PcP is not. Such vertical stretching can be readily envisaged in the arc setting of Honshu where these observations are most evident.

4. Discussion and conclusions

An abundant record of PcP and PKiKP travel times and amplitudes observed at numerous seismic stations from two events was collected. PcP and/or PKiKP waves were observed from a single earthquake and a nuclear explosion on about 70 stations. We found a general strong negative correlation in the detection of PcP and PKiKP waves, which has not been previously reported. We exclude the possibility that the negative correlation pattern stems from the source radiation pattern. Although core–mantle boundary structure can significantly contribute to the scatter in ratio of PKiKP/PcP, it cannot explain a more systematic negative correlation in PKiKP and PcP detections. We conclude that the volumetric heterogeneity in the crust and upper mantle on the receiver side must be the cause of the observed spatial coherence in anti-correlation of PKiKP and PcP detections. It is possible to deduce from the angular decorrelation between PKiKP and PcP that an important characteristic wavelength of the heterogeneity must be on the order of 10–30 km, which is also a function of the depth of these structures, not well constrained with our observations. This wavelength of heterogeneity is in agreement with the results of recent numerical simulations carried out to explain long, high frequency coda of P and S waves recorded in northern Australia (Kennett and Furumura, 2008).

The role of heterogeneity in modifying weak signals is complex. Although it may not seem physically intuitive that suitable stochastic heterogeneity can produce a consistent pattern for signals traveling at slightly different angles to the vertical, angular decorrelation in amplitude and phase is well recognized in scattering studies for quite small changes in propagation direction (e.g., Wu and Flatté, 1990). This factor contributes to the specific amplitudes encountered for the phases. Since both signals are weak it does not require much adverse circumstance for one to be suppressed while the other is still visible.

Earth's lithosphere and asthenosphere are very heterogeneous, as they consist of plate fragments of various ages, thicknesses and melting points (e.g., Anderson, 2006; Thybo and Anderson, 2006). Delaminated lower continental crust can consist of large chunks of eclogite. Melts from recycled oceanic crust can exist beneath the lithosphere. Regardless of their source, partial melt pockets or lenses could also be a generator of the observed anti-correlation. In a recent study of the podal PKPPKP waves, Tkalčić et al. (2006) invoked the existence of small-scale chemical heterogeneity or lenses of partial melt in the upper mantle between the depths of 150–220 km to explain the precursors to PKPPKP waves by backscattering. Thin lenses of melt can certainly increase scattering and affect amplitudes, but this type of model can trade off with simpler heterogeneous models with only just slightly higher levels of percent perturbations in velocities and densities. It is difficult to distinguish between the two possibilities without independent types of observations. Recently, Davies (in press) has presented a geochemical argument that while a partial melt might be observed at the surface only in extreme conditions, a connected network of grain-scale melt channels, porous flow and the possible formation of macroscopic high-flux channels might be widely present in the upper mantle in conjunction with the difficulty of extracting partial melt from eclogite bodies.

This mechanism in the crust and upper mantle together with lateral variations in the lowermost mantle explains the large scatter previously observed in PKiKP/PcP amplitude ratios studies (e.g., Koper and Dombrovskaya, 2005) and in absolute amplitudes of PKiKP or PcP waves plotted as a function of epicentral distance. These effects have a profound and destructive impact on our analysis and understanding of the ICB density contrast from body waves. Heterogeneity on the receiver side would efficiently shut down any portion of energy that remained of PKiKP waves by the time they almost reached the receiver, and only in rare cases where both PcP and PKiKP escape this obstacle or are affected by a similar amount, would we get reliable information about their amplitudes and hence the ICB density contrast. The magnitude of this density contrast contributes to the energy available for a dynamo driven by compositional convection (Gubbins et al., 2004). Our interpretation of the fluctuations of the PKiKP/PcP ratio used to infer this density contrast suggests that any reduction of its global error bounds will require both improved resolution of 3D structure at 100–1000 km scale lengths near the CMB and ICB as well as knowledge of small scale (1–10 km) statistically described structure in the crust and upper mantle.

Acknowledgements

V.F. Cormier's participation was supported by a grant from the Vice Chancellor of the Australian National University funding travel as a Visiting Fellow, and by the National Science Foundation under grant EAR 07-38492. We are grateful to two anonymous reviewers, whose comments helped to improve the manuscript.

References

Aki, K., 1973. Scattering of P waves under the Montana LASA. J. Geophys. Res. 78, 1334–1346.
Anderson, D.L., 2006. Speculations on the nature and cause of mantle heterogeneity. Tectonophysics 416, 7–22.
Červený, V., 2001. Seismic Ray Theory. Cambridge Univ. Press, Cambridge, 713 pp.
Cormier, V.F., 1986. An application of the propagator matrix of dynamic ray tracing: the focusing and defocusing of body waves by three-dimensional velocity structure in the source region. Geophys. J. R. Astr. Soc. 87, 1159–1180.
Cormier, V.F., 2000. D″ as a transition in the heterogeneity spectrum of the lowermost mantle. J. Geophys. Res. 105, 16193–16205.
Davies, G., in press. Inefficient melt extraction from a heterogeneous, mildly depleted mantle: no hidden reservoir, G-cubed.
Flatté, S.M., Wu, R.S., 1988. Small-scale structure in the lithosphere and asthenosphere deduced from arrival-time and amplitude fluctuations at NORSAR. J. Geophys. Res. 93, 6601–6614.
Gubbins, D., Alfe, D., Masters, G., Price, G.D., Gillan, M., 2004. Gross thermodynamics of two-component core convection. Geophys. J. Int. 157, 1407–1414.
Kennett, B.L.N., Furumura, T., 2008. Stochastic waveguide in the lithosphere: Indonesian subduction zone to Australian craton. Geophys. J. Int. 172, 363–382.
Koper, K.D., Dombrovskaya, M., 2005. Seismic properties of the inner core boundary from PKiKP/P amplitude ratios. Earth Planet. Sci. Lett. 237, 680–694.
Li, X.D., Romanowicz, B., 1996. Global mantle shear-velocity model developed using nonlinear asymptotic coupling theory. Geophys. J. Int. 101, 21245–22272.
Menke, W., 1986. Few 2–50 km corugations on the core mantle boundary. Geophys. Res. Lett. 13, 1501–1504.
Sato, H., Fehler, M., 1998. Seismic Wave Propagation and Scattering in the Heterogeneous Earth. Am. Inst. Phys. Press.
Shearer, P.M., Masters, T.G., 1990. The density and shear velocity contrast at the inner core boundary. Geophys. J. Int. 102, 491–498.
Souriau, A., Souriau, M., 1989. Ellipticity and density at the inner core boundary from subcritical PKiKP and PcP data. Geophys. J. Int. 98, 39–54.
Sze, E., Van der Hilst, R.D., 2003. Core mantle boundary topography from short period PcP, PKP, and PKKP data. Phys. Earth Planet. Int. 135, 27–46.
Thorne, M.S., Garnero, E.J., 2004. Inferences on ultra-low velocity zone structure from global analysis of SPdKS waves. J. Geophys. Res. 109, B08301, doi:10.1029/2004JB003010.
Thybo, H., Anderson, D.L., 2006. The heterogeneous mantle. Tectonophysics 416, 1–6.
Tkalčić, H., Kennett, B.L.N., Cormier, V.F., 2009. On the inner–outer core density contrast from PKiKP/PcP amplitude ratios and uncertainties caused by seismic noise. Geophys. J. Int., doi:10.1111/j.1365-246X.2009.04294.x.
Tkalčić, H., Flanagan, M., Cormier, V.F., 2006. Observations of near-podal P'P' precursors: evidence for back scattering from the 150–220 km zone in Earth's upper mantle. Geophys. Res. Lett. 33, L03305, doi:10.1029/2005GL024626.
Tkalčić, H., Romanowicz, B., 2002. Short scale heterogeneity in the lowermost mantle: insights from PcP-P and ScS-S data. Earth Planet. Sci. Lett. 201, 57–68.
Tkalčić, H., Romanowicz, B., Houy, N., 2002. Constraints on D″ structure using PKP(AB-DF), PKP(BC-DF) and PcP-P traveltime data from broad-band records. Geophys. J. Int. 148, 599–616.
Wu, R.-S., Flatté, S.M., 1990. Transmission fluctuations of seismic waves across seismic arrays. In: Wu, Aki (Eds.), Seismic Wave Scattering and Attenuation. Pure Appl. Geophys. 132, 175–196.
Zheng, Y., Wu, R.-S., 2008. Theory of transmission fluctuations in random media with a depth-dependent background velocity structure. Adv. Geophys., Ch. 2.